Cancer Cell
Article

Metastatic Colonization Requires the Repression of the Epithelial-Mesenchymal Transition Inducer Prrx1

Oscar H. Ocaña,[1] Rebeca Córcoles,[1,5] Ángels Fabra,[2,5] Gema Moreno-Bueno,[3,4] Hervé Acloque,[1,6] Sonia Vega,[1] Alejandro Barrallo-Gimeno,[1,7] Amparo Cano,[3] and M. Angela Nieto[1,*]
[1]Instituto de Neurociencias CSIC-UMH, Avda. Ramón y Cajal s/n, 03550 San Juan de Alicante, Spain
[2]IDIBELL (Bellvitge Biomedical Research Institute), Centre d' Oncologia Molecular, Gran Via de L'Hospitalet, 199 Barcelona, Spain
[3]Departamento de Bioquímica, UAM. Instituto de Investigaciones Biomédicas "Alberto Sols" CSIC-UAM, IdiPAZ, Arturo Duperier, 4, 28029 Madrid, Spain
[4]Fundación MD Anderson Internacional, Arturo Soria 270, 28033 Madrid, Spain
[5]These authors equally contributed to this work
[6]Present address: UMR 444, INRA-ENVT, Génétique Cellulaire, F-31706 Toulouse, France
[7]Present address: Deptartamento de Ciències Fisiològiques - II, Facultat de Medicina i Odontologia, Universitat de Barcelona, Feixa Llarga, s/n, 08907 L'Hospitalet Llobregat, Barcelona, Spain
*Correspondence: anieto@umh.es
http://dx.doi.org/10.1016/j.ccr.2012.10.012

SUMMARY

The epithelial-mesenchymal transition (EMT) is required in the embryo for the formation of tissues for which cells originate far from their final destination. Carcinoma cells hijack this program for tumor dissemination. The relevance of the EMT in cancer is still debated because it is unclear how these migratory cells colonize distant tissues to form macrometastases. We show that the homeobox factor Prrx1 is an EMT inducer conferring migratory and invasive properties. The loss of Prrx1 is required for cancer cells to metastasize in vivo, which revert to the epithelial phenotype concomitant with the acquisition of stem cell properties. Thus, unlike the classical EMT transcription factors, Prrx1 uncouples EMT and stemness, and is a biomarker associated with patient survival and lack of metastasis.

INTRODUCTION

Metastasis is still the cause of 90% of deaths from carcinomas (Gupta and Massagué, 2006) and despite the efforts devoted to understand the mechanisms that drive disseminated tumor cells to colonize distant tissues, it remains the least understood step of tumor progression. To form distant metastasis, cancer cells must first dissociate from the primary tumor, invade adjacent tissues, and intravasate into lymphatic and blood vessels to later colonize lymph nodes and distant organs. For invasion to occur, there is evidence that carcinoma cells can undergo a phenotypic transformation, the epithelial-mesenchymal transition (EMT; Nieto, 2011), which enables them to invade, intravasate, and navigate through a network of thin vessels while acquiring stem cell-like properties (Mani et al., 2008; Morel et al., 2008; Wellner et al., 2009). Still, it is not clear how these individual mesenchymal cells can then form distant macrometastases, in particular because carcinoma metastases usually present a well-differentiated epithelial phenotype. Clues as to how this mesenchymal-to-epithelial plasticity may arise have come from the study of embryonic development, where several rounds of EMT and the reverse process, mesenchymal-epithelial transition (MET), are responsible for the formation of many tissues and organs (Yang and Weinberg, 2008; Thiery et al., 2009). Indeed, although experimental evidence is still scarce, some indications suggest that this might indeed occur in vivo

Significance

Metastasis is the cause of the vast majority of cancer-associated deaths, but the underlying mechanisms remain poorly understood. The invasion and dissemination steps during carcinoma progression have been associated with EMT, which endows cells with invasive abilities and the stem cell-like properties required to initiate the formation of a secondary tumor. However, it is unclear how these migratory cells colonize distant territories. Here, we show that abrogation of the EMT is important for metastatic colonization. The loss of the EMT inducer Prrx1 allows cancer cells to revert EMT while acquiring tumor-initiating abilities. Our results help reevaluate the potential benefits of current therapeutic strategies aimed at targeting the EMT while supporting those aimed at targeting stem cell properties in cancer cells.

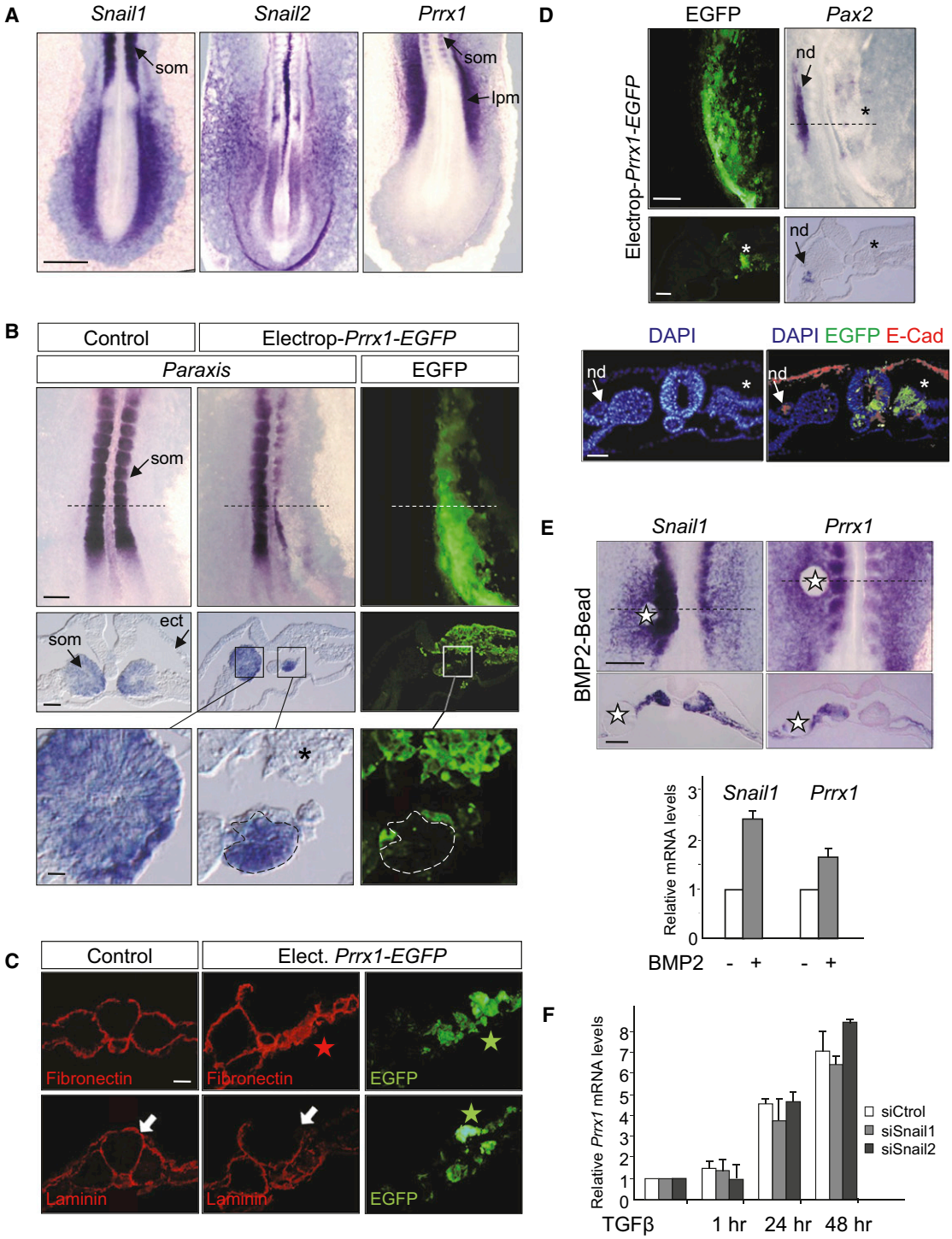

Figure 1. The Prrx1 Transcription Factor Induces a Full EMT In Vivo

(A) Dorsal view of the posterior region of stage HH10-11 chick embryos. The expression of *Snail1*, *Snail2*, and *Prrx1* was detected by ISH. Note the complementary expression patterns. Lpm, lateral plate mesoderm; som, somites. Scale bar: 500 μm.

(B) Chick embryos were coelectroporated on the right hand side with an EGFP expressing construct and a vector expressing *Prrx1* or an empty control vector at stage HH4 and examined at stage HH10-11. The expression of *Paraxis* was detected by ISH and the expression of EGFP by immunofluorescence staining. Top panels show the dorsal views and the middle panels show transverse sections taken at the level of the dotted lines after the ectopic expression of Prrx1. The bottom panels show high power images of boxed areas. Note that the loss of the epithelial somite marker *Paraxis* (black asterisk) occurs only in the electroporated (EGFP) cells. Ect, ectoderm.; Som, somites Scale bars: 250, 50, and 10 μm for upper, middle, and lower panels, respectively.

(C) Expression of fibronectin and laminin and EGFP detection in transverse frozen sections of chick embryos electroporated with *Prrx1* or the control vector. Note the excess of fibronectin (red star) and the disruption of the basement membrane (white arrows) in the electroprated areas (green stars). Scale bar: 50 μm.

during tumor progression (Chaffer et al., 2006; Dykxhoorn et al., 2009).

The similarities between developmental and pathologic EMT validate the embryo as an excellent model to find new clues regarding the events driving tumor progression. Indeed, the EMT has developed during evolution to allow cells to migrate to their final target destination, which they colonize before contributing to the formation of definitive differentiated organs (Nieto and Cano, 2012), a concept very similar to the process of metastatic colonization. Therefore, the reactivation of a developmental program such as the EMT can make tumor cells competent to respond to internal and external cues that confer them with a high degree of epithelial plasticity. The aim of this study was to take advantage of the vertebrate embryo to get further insight into the mechanisms of metastatic colonization, focusing on epithelial plasticity and the acquisition of stem cell properties.

RESULTS

Prrx1 Induces Full EMT in Embryos and Cancer Cells

In search for EMT inducers, we performed expression screening for transcription factors associated with early mesodermal tissues in the chick embryo. We previously showed that upon delamination from the primitive streak, the subdivision of mesodermal territories was accompanied by the distribution of *Snail1* and *Snail2* expression (Sefton et al., 1998). However, we have now found a subset of lateral plate mesodermal cells that did not express either *Snail1* or *Snail2*, but rather express the paired-related homeobox transcription factor *Prrx1* (Figure 1A). *Prrx1* is also expressed in the somites. Interestingly, the somites also express *Snail* genes but, as in the lateral plate mesoderm, they also show complementary expression patterns (Figure S1A).

Prrx1 had previously been implicated in several developmental processes and aspects of fibroblast behavior (Cserjesi et al., 1992; McKean et al., 2003), we therefore examined whether Prrx1 could be an EMT inducer. Ectopic expression of Prrx1 in the chicken embryo, as Snail1, caused failure of epithelial somite development, as assessed by morphology and by the loss of expression of the somitic epithelial markers *Paraxis* (Figures 1B and S1B) and *Uncx4.1* (Figure S1C). This defective epithelialization occurred in a cell autonomous manner (Figure 1B) and was accompanied by the increase in fibronectin deposition and the disappearance of the basement membrane as assessed by laminin staining (Figure 1C), all hallmarks of an EMT.

In addition to the paraxial (somitic mesoderm), *Prrx1* ectopic expression also prevented the epithelialization of the intermediate mesoderm precluding the formation of its derivative, the nephric duct (nd), as assessed by morphologic analysis and by the absence of expression of both its specific marker *Pax2* (Figure 1D, upper panels) and of the epithelial marker E-cadherin (Figure 1D, lower panels).

Like *Snail1*, *Prrx1* expression was induced by BMP2 in the embryo (Figure 1E) and ectopic expression of either *Snail1* or *Prrx1* did not influence that of the other gene (Figure S1D). Therefore, BMP2 seems to induce Snail1 and Prrx1 in an independent manner. The existence of two parallel activation pathways triggered by members of the tumor growth factor (TGF)-β superfamily was confirmed in MDCK cells after treatment with TGF-β, the main inducer of EMT transcription factors in epithelial cells (EMT-TFs; Thiery et al., 2009). Accordingly, interfering with Snail1 or Snail2 expression in MDCK cells did not prevent the induction of *Prrx1* by TGF-β (Figure 1F).

Because TGF-β could induce *Prrx1* expression in MDCK cells, we examined whether *Prrx1* could induce EMT in these cultured cells. Indeed, *Prrx1*-expressing MDCK cells adopted a mesenchymal morphology concomitant with loss of E-cadherin expression and gain of vimentin (Figure 2A). In cultured wound-healing assays, these MDCK-Prrx1 cells healed the wound much faster than control cells (Figure 2B) and they could migrate through collagen gels (Figure 2C). Unlike MDCK-mock cells that formed prototypical epithelial ducts, MDCK-Prrx1 cells grown in 3D matrigel cultures instead formed a network of mesenchymal cells (Figure 2D). Moreover, these cells had downregulated epithelial markers and they had gained the expression of mesenchymal markers, including some EMT-TFs (Figure 2E). Interestingly, as already observed in living embryos, Prrx1 did not influence *Snail1* expression, as MDCK-Prrx1 cells are devoid of *Snail1* transcripts (Figure 2E).

Given the relationship between EMT and Prrx1, we analyzed the expression of this factor in a panel of human cancer cell lines and we found that it was associated with the mesenchymal phenotype and invasive properties (Figures 2F and S2). Furthermore, when compared to the expression of other EMT-TFs in these cell lines, we noted that *PRRX1* expression was frequently associated with that of *TWIST1* in invasive cell lines, indicating that both factors could cooperate in the induction of EMT (Figures 2F and S2; data not shown).

To further characterize Prrx1 as an EMT inducer in vivo and to explore its relationship with Twist1, we moved to the zebrafish embryo, which is very amenable to gain and loss of function studies. We found that among the Prrx and Twist family members in the fish, *prrx1a* and *twist1b* show an expression pattern very similar to that observed in the chick for *Prrx1* and *Twist1*. In particular, these two genes were also coexpressed in the lateral plate mesoderm (lpm) (Figures 3A and 3B). The

(D) Prrx1 electroporation was carried out as in (B). Upper panels show the expression of *Pax2* detected by ISH. Note the absence of *Pax2* on the right hand side (asterisk), more evident on the sections (middle panels). The bottom panels show DAPI stainings (blue) to visualize nuclei and E-cadherin detected by immunofluorescence (red). Note the presence of the epithelial nephric duct (nd) at the left side but it is missing at the right side (asterisk). Scale bars: 500 μm (upper and middle panels) and 50 μm (bottom panels).

(E) BMP2-soaked beads (white stars) were implanted in the left lpm of chick embryos at stage HH7 that were examined 5 hr later. Note both in the whole mounts and in the sections that the expression of *Snail1* and *Prrx1* is stronger and expanded close to the beads. The bar graph shows the result of real-time RT-PCR (bottom). Scale bars: 250 μm (upper panels) and 100 μm (lower panels).

(F) The expression of *Prrx1* in TGF-β-treated MDCK cells transfected with the indicated siRNAs was measured by real-time PCR analysis.

Histograms in (E) and (F) show one representative of three independent experiments and include the mean ± SD of technical triplicates.

See also Figure S1.

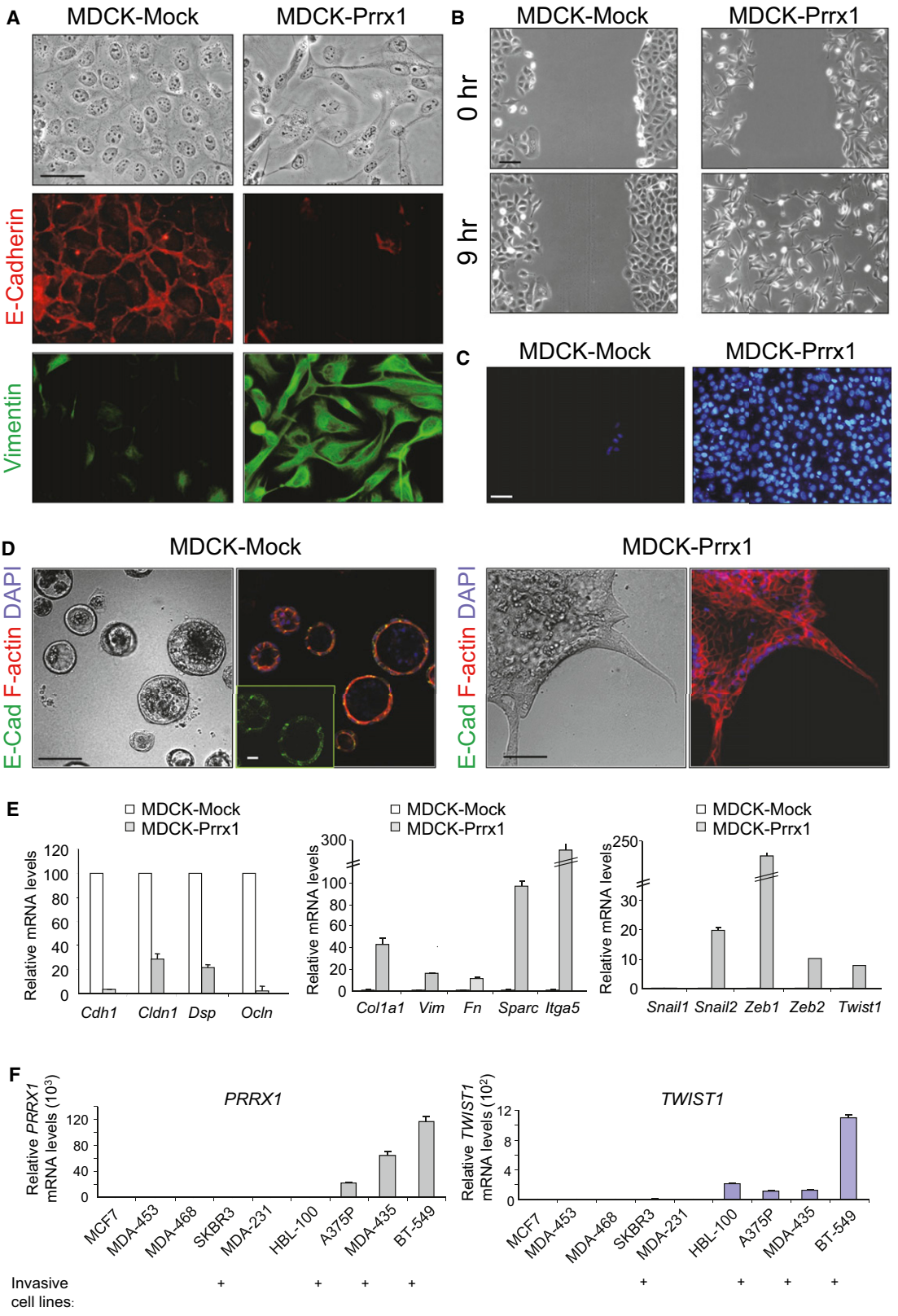

Figure 2. Prrx1 Induces a Full EMT in MDCK Cells Concomitant with the Acquisition of Migratory and Invasive Properties

(A) Phase-contrast images and images of immunofluorescence staining of indicated proteins of MDCK clones expressing Prrx1 or an empty vector (mock). Scale bar: 50 μm.

gain of function induced by injecting *prrx1a* mRNA into embryos produced a dramatic phenotype, whereby lpm cells became invasive and violated the embryonic boundaries to enter the extraembryonic tissues. The position of the cells could be readily detected by examining the expression of *twist1b*, with cells found all around the yolk (Figure 3C, lower panels). Knockdown of *prrx1a* by antisense morpholino oligonucleotide (MO) injection (*prrx1a*^{MO1}) produced the opposite effect to that of *prrx1a* mRNA injection, with cells being retained very close to the neural tube, failing to migrate and colonize their normal territory (Figure 3D; see also Figure S3 for morpholino specificity and efficiency). A different MO against *prrx1a* (*prrx1a*^{MO2}, see Figure S3) was also tested giving similar results (not shown). We decided to continue our experiments with MO1, which will be hereafter referred to as *prrx1a*^{MO}. The observed defects were specific to Prrx1a silencing as this phenotype could be rescued by coinjection of *prrx1a*^{MO} and *prrx1a*^{mRNA} (Figures 3E and 3G). Interestingly, injection of *twist1b*^{MO} could also rescue the Prrx1a overexpression phenotype, suggesting that these genes cooperate to induce the invasive phenotype observed in the lpm, the tissue in which they are coexpressed (Figures 3F and 3G). Indeed, this is compatible with the finding that tissues other than the lpm did not seem to be affected when *prrx1a* alone was overexpressed (Figure 3C; *prrx1a*^{mRNA}). These results indicate that Prrx1a also behaves as an EMT inducer in the fish embryo and that its upregulation induces a prominent invasive phenotype in vivo when acting in cooperation with Twist1b.

To further investigate the cooperation between Prrx1 and Twist in conferring invasive properties, we examined the effect of their downregulation in the invasive BT-549 human cancer cell line, which expresses significant levels of both factors (Figure 2F) and lacks SNAI1 expression (Moreno-Bueno et al., 2011). We found that transient RNA interference of *PRRX1* or *TWIST1* compromised the ability of BT-549 cells to degrade collagen, which was further diminished when both factors were knocked-down simultaneously (Figure 3H). Three independent siRNA sequences were tested in these experiments (not shown). Conversely, in the TWIST1-positive, PRRX1-negative, and noninvasive HBL-100 cells, *PRRX1* transfection renders them invasive, a phenotype that was diminished when the endogenous expression of *TWIST1* was downregulated (Figure 3I). Together, our data indicate that PRRX1 also confers invasive properties to cancer cells in cooperation with TWIST1.

Cells Must Lose Prrx1 to Metastasize

We next investigated the role of Prrx1 in tumorigenesis by injecting MDCK-Prrx1 and control cells into the tail vein of immunocompromised mice and we failed to detect metastatic lung foci (not shown). Moreover, when PRRX1-positive BT-549 breast tumor cells were similarly injected, we did not detect lung colonization either (Figure 4A; shC). However, when PRRX1 was stably silenced by short-hairpin interference mediated by lentiviral infection, BT-549 cells consistently colonized the lung in all animals, inducing metastatic foci (Figure 4A; shPR1). Likewise, silencing both PRRX1 and TWIST1 in BT-549 cells induced lung metastasis in 100% of animals and the number of foci increased significantly (Figure 4A; shPR1-shTW1), indicating that TWIST1 downregulation also favors metastasis formation. However, TWIST1 silencing alone (shTW1) was not sufficient to induce metastatic colonization in the presence of PRRX1 (Figure 4A). The lack of colonization of control or shTWIST1 cells was not due to a failure in extravasation, since single GFP-positive cells were detected 24–30 hr after intravenous injection in the lung parenchyma in all conditions (Figure S4A). Quantification of GFP-positive lesions in the lungs at necropsy on day 60 together with a fluorescence and histologic analysis confirmed the presence of metastasis in mice injected with BT-549 cells knocked-down for PRRX1 alone or for PRRX1 and TWIST1, together with the absence of metastasis in mice injected with control cells or knocked-down for TWIST1 alone (Figure 4B). Interestingly, cardiac and mediastinal metastasis were also observed at necropsy in one mouse in which both PRRX1 and TWIST1 were downregulated (Figure S4B). Cells in which PRRX1 alone was silenced still express TWIST1 (Figure S4C), indicating that PRRX1 silencing in BT-549 cells is sufficient for these cells to engraft the lung and therefore, for colonization in experimental metastasis assays.

To test the role of PRRX1 in primary tumor formation and in distant metastatic colonization in vivo, we orthotopically implanted the BT-549 cells into the right and left inguinal mammary fat pads of athymic nude mice. The generation of primary tumors closely paralleled the capacity of these cells to metastasize in the previous experiments. Thus, while BT-549 control cells or those in which only TWIST1 was downregulated never generated tumors, downregulation of PRRX1 and TWIST1 or even of PRRX1 alone was sufficient to enable tumor growth (Figure 4C). The tumors that developed in mice bearing BT-549 cells lacking both PRRX1 and TWIST1 were detected earlier than those with PRRX1-defective BT-549 cells, although the growth rate was similar in both cases (not shown). Primary tumors were always confined to the mammary gland, with the fatty tissue facing the tumor being almost intact and with a remarkable absence of invasive cells at the tumor margin (Figure 4D). Consistent with their deficient invasive ability (Figure S4D), no metastatic foci

(B) The migratory properties of MDCK-Prrx1 cells were tested in wound healing assays. Scale bar: 100 μm.
(C) Invasive behavior of MDCK-Prrx1 cells in collagen-type-IV gels, as observed in Boyden chamber invasion assays. Nuclei of invasive cells are visualized with DAPI. Scale bar: 100 μm.
(D) Phase-contrast images showing the morphology of control and Prrx1-expressing MDCK cells in 3D culture. Cells were stained with phalloidin for F-actin and E-cadherin (E-Cad) antibodies, and counterstained with DAPI. Scale bar: 50 μm (main pictures) and 15 μm (inset).
(E) Real-time RT-PCR analysis of control and Prrx1-expressing MDCK cells show the repression of epithelial markers genes (*Cdh1, E-cadherin*; *Cldn1*, *claudin 1*; *Dsp*, *desmoplakin*; and *Ocln*, *occludin*) and the activation of mesenchymal markers (*Col1a1*, *collagen I*; *Vim*, *vimentin*; *Fn*, *fibronectin*; *Sparc;* and *Itga5*, *integrin* α*5*) together with several EMT-TFs (*Snail1, Snail2, Zeb1, Zeb2*, and *Twist1*) upon Prrx1 ectopic expression.
(F) Expression of *PRRX1* and *TWIST1* in a panel of human cancer cell lines and its relationship with invasive properties.
Histograms in (E) and (F) show one representative of three independent experiments and include the mean ± SD of technical triplicates.
See also Figure S2.

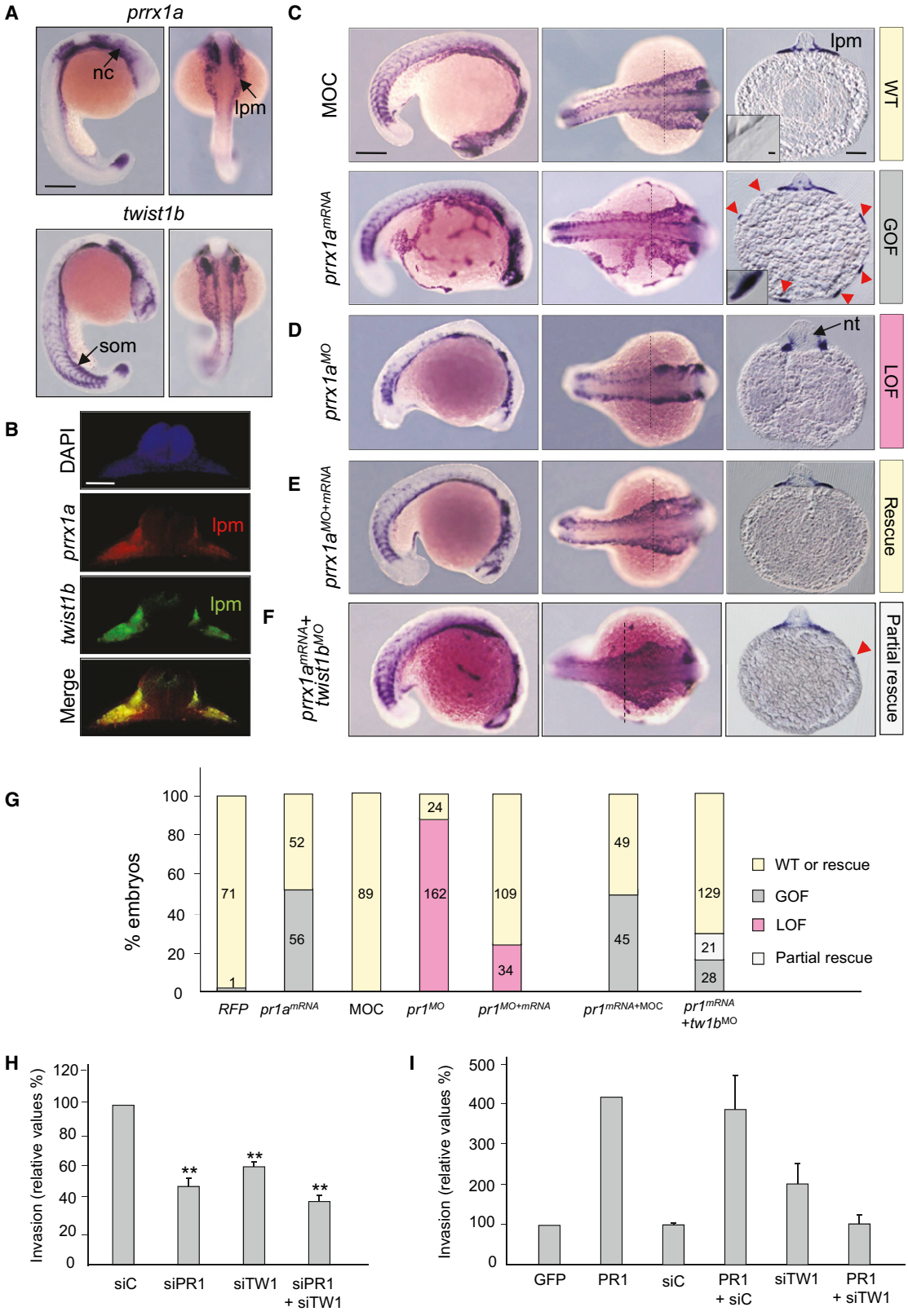

Figure 3. Prrx1 Overexpression Induces Massive Invasion in Zebrafish Embryos

(A) Expression of *prrx1a* and *twist1b* in zebrafish embryos at the 22-somite stage (lateral and dorsal views). nc, neural crest; lpm, lateral plate mesoderm; som, somites. Scale bar: 200 μm.

were detected in any organ at necropsy, even 4 months after inoculation of BT-549 cells where PRRX1 alone or PRRX1 and TWIST1 were downregulated. This is again reminiscent of the situation in embryos, where PRRX1 loss prevents cells from migrating to then colonize their normal territories. Interestingly, metastatic growth was found in axillary lymph nodes in two out six mice bearing BT-549 PRRX1- and TWIST1-deficient cells (Figure 4C), compatible with the proposal that lymph node colonization does not require EMT. As such, although individual mesenchymal cells can invade lymph nodes, their colonization can also occur through collective cell migration (Giampieri et al., 2009).

The Loss of PRRX1 Reverts EMT and Induces Stem Cell Properties

Having shown that the loss of PRRX1 was sufficient for metastatic colonization, but that PRRX1 expression was important for invasion, we examined the impact of its downregulation on the behavior of cancer cells. We first found that the loss of PRRX1 was indeed sufficient for BT-549 cells to revert EMT, undergoing a MET in culture, evidenced by the changes in morphology and actin filament reorganization (Figure 5A). When grown in 3D Matrigel cultures, PRRX1-deficient BT-549 cells did not form mesenchymal networks like control cells, but rather they formed spheroids that had lost vimentin expression, expressed significant levels of E-cadherin and β-catenin at the cell membrane and that secreted laminin I, indicative of the formation of a basement membrane-like structure (Figure 5B). A similar phenotype was observed in cells in which both PRRX1 and TWIST1 were downregulated (Figure 5B). However, TWIST1 downregulation in BT-549 cells was unable to revert the EMT (Figure 5B). It is worth noting here that these cells still express high levels of PRRX1 (Figure S4C). In summary, it appears that the loss of PRRX1 is sufficient to revert the EMT, even in the presence of other EMT inducers such as TWIST1.

We next asked whether the altered phenotype and the ability of BT-549 cells to form metastasis in vivo following *PRRX1* loss was at least partially due to a modification in the tumor-initiating properties of the nontumorigenic BT-549 cells. Soft agar cultures and mammosphere formation assays in ultralow attachment plates were used to examine the cells' ability to support attachment-independent growth and to self-renew, respectively, taken as indicators of tumor-initiating capacity. While BT-549 control cells were unable to grow in soft agar, silencing of *PRRX1* or of both *PRRX1* and *TWIST1* enabled these cells to form colonies (Figures 6A and 6B), and facilitated secondary mammosphere formation (Figures 6C and 6D). The number of mammospheres increased when *TWIST1* was additionally silenced, compatible again with a cooperation between these two factors. However, TWIST1 downregulation alone was not able to induce BT-549 cells to grow in soft agar or to form mammospheres (Figures 6A–6D). This is compatible with the previous finding that TWIST1 expression can endow cells with stem cell properties (Mani et al., 2008; Morel et al., 2008). Importantly, PRRX1 loss was sufficient to sustain mammosphere growth up to at least six consecutive passages (not shown).

It has been shown that EMT inducers attenuate proliferation, which may also compromise tumor growth (Vega et al., 2004; Mejlvang et al., 2007). Similarly, we found that PRRX1 loss enhanced cell division, like Snail1 loss, as evident both by the increase in cell number and the expression of the mitotic marker phospho-histone 3 (PH3; Prigent and Dimitrov, 2003) (Figures 6E and 6F). A similar effect was observed when both PRRX1 and TWIST1 were silenced. Again, in the presence of PRRX1, TWIST1 downregulation was not able to significantly alter cell growth (Figures 6E and 6F).

To further characterize the impact of PRRX1 loss, we examined the expression of the CD44 and CD24 cell surface markers, given that their relative expression and the $CD44^{high}/CD24^{low}$ profile in particular, has been associated with stemness in both normal mammary and breast cancer cells (Sleeman et al., 2006). Silencing PRRX1 or PRRX1 and TWIST1 converted BT-549 cells (mostly $CD44^{+}/CD24^{+}$ double-positive) into $CD44^{high}$ cells (Figure 6G), indicative of a stem cell phenotype (Marotta et al., 2011). Therefore, PRRX1 downregulation was sufficient to shift cells toward a population of $CD44^{+}$ single-positive cells. By contrast, TWIST1 downregulation decreased CD44 expression. As CD24 was almost abrogated from the cell surface after PRRX1 silencing, we wondered whether PRRX1 could regulate its expression. We found that PRRX1 loss leads to an almost complete downregulation of *CD24* transcription. By contrast, TWIST1 downregulation increases the levels of *CD24* transcripts, pointing again to an antagonistic role between PRRX1 and TWIST1 in relation to the acquisition of stem cell properties (Figure 6H).

If PRRX1 loss is sufficient to induce stem cell properties in a non-tumorigenic cell line, ectopic expression of PRRX1 in tumorigenic PRRX1-negative cells may have a negative impact on their stem cell properties. To test it, we chose the tumorigenic and highly metastatic MDA-MB-231 cell line (from now on

(B) Double fluorescent ISH of transverse gelatin sections taken at the mid trunk level shows the coexpression of *prrx1a* and *twist1b* in the lpm. Scale bar: 50 μm. (C–F) ISH for *twist1b* to detect lpm cells in zebrafish embryos. Lateral (left), dorsal (middle), and transverse gelatin sections (at the level of the dotted lines, right) view of lpm cells of zebrafish embryos microinjected with a control morpholino (MOC) or *prrx1a* mRNA ($prrx1a^{mRNA}$) (C), a *prrx1a* morpholino oligonucleotide ($prrx1a^{MO}$) (D), $prrx1a^{mRNA}$ together with $prrx1a^{MO}$ (E), or $twist1b^{MO}$ together with $prrx1a^{mRNA}$ (F). nt, neural tube. Red arrowheads indicate invasive cells in extraembryonic territories. A color code was assigned to the different phenotypes (boxes on the right) as follows: yellow, WT (wild-type) and rescue; gray, GOF (gain of function); pink, LOF (loss of function/knockdown), pale gray, partial rescue. This color code was also used for the quantification of phenotypes shown in (G), Scale bar: 200 μm in left and middle, 100 μm in the right, and 10 μm in the insets.

(G) Quantitative analysis of the fish phenotypes shown in (C–F) and that of microinjection of a control mRNA (*RFP*). (H) Invasive properties of BT-549 human cancer cells after transient downregulation of *PRRX1* and/or *TWIST1* by siRNA transfection. Invasion is represented relative to that observed in control (siC-treated) BT-549 cells. Histograms represent the mean ± SD of three independent experiments (**$p < 0.01$ compared to the control condition).

(I) Analysis of cell invasion of collagen matrices after ectopic PRRX1 expression (PR1) and/or downregulation of endogenous TWIST1 expression (siTW1) in HBL-100 cells. Histograms represent the mean ± SD of four independent experiments ($p = 0.083$ PR1+siC versus siC; $p = 0.082$ PR1+siTW1 versus PR1+siC). PR or pr, PRRX or prrx; TW or tw, TWIST1 or twist, respectively.

See also Figure S3.

A

BT-549 cells	Inoculation	n mice	Sacrifice	Lung Metastatic Colonization	number of foci /single mice
shC	iv	11	60 days	none	none
shPR1	iv	9	60 days	100 %	1-12
shPR1-shTW1	iv	10	60 days	100 %	17-40
shTW	iv	10	60 days	none	none

B

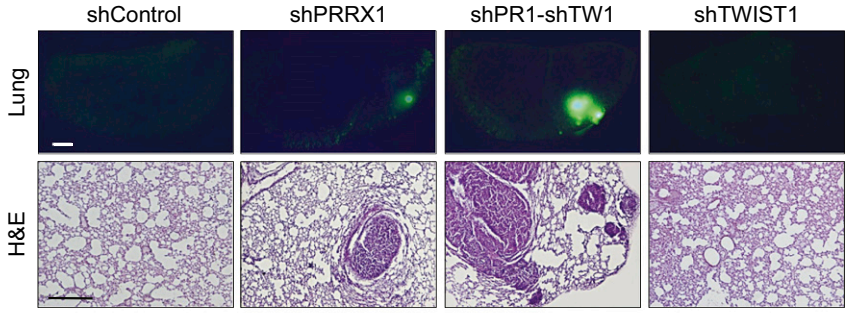

C

BT-549 cells	Inoculation	n mice	Tumor detection	Tumor development Incidence	Lymph node Incidence
shC	i.m.f.p.	3 double injections	none (0/6) at 138 days	none	none
shPR1	i.m.f.p.	3 double injections	day 31-40 (6/6)	100 %	none (0/6) at 138 days
shPR1-shTW1	i.m.f.p.	6 double injections	day 21-29 (11/12)	91.6 %	2/6 at 90 days
shTW1	i.m.f.p.	3 double injections	none (0/6) at 138 days	none	none

D

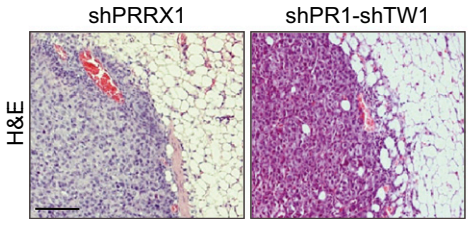

Figure 4. PRRX1 Expression Regulates the Tumorigenic and Metastatic Potential

(A) Experimental lung metastasis in Balb/c nude mice 60 days after injection of BT-549 cells.

(B) Representative GFP-positive foci in lungs (upper panels) and H&E sections of the lungs (lower panels). Scale bars: 1 mm (upper panels) and 200 μm (lower panels).

(C) Primary xenografts generated from BT-549 cells on the days indicated after double inguinal intramammary fat pad (i.m.f.p.) injection (1×10^6 cells/injection site).

(D) Representative H&E sections of tumors from mice injected with BT-549 shPRRX1 (left) or shPRRX1-shTWIST1 cells (right). Scale bar: 100 μm.

C, control; PR, PRRX; TW, TWIST.

See also Figure S4.

MDA-231), which expresses EMT-TFs but is devoid of PRRX1 and TWIST1 (Figures 2F and S2). As expected, stable PRRX1 ectopic expression in MDA-231 cells alone or together with TWIST1 (Figure 7A) did not have any impact on the morphology of these already mesenchymal cells (Figure 7B). However, both the number of colonies formed in soft agar cultures and particularly, the number of secondary and tertiary mammospheres significantly decreased upon PRRX1 ectopic expression (Figures 7C–7F). Interestingly, all these effects were reinforced by the additional ectopic expression of TWIST1 (Figures 7C–7F). Furthermore, MDA-231 cells (mostly $CD44^+$ single positive) lose CD44 expression and shift toward a $CD44^-/CD24^-$ double-negative population (Figure 7G). Hence, as hypothesized, the effect of ectopically expressing PRRX1 in MDA-231 cells is opposite to that found after PRRX1 downregulation in BT-549 cells.

Collectively, our data indicate that the loss of PRRX1 alone is sufficient to revert EMT, inducing a MET accompanied by the acquisition of stem cell properties and increased proliferation, all important events for metastatic colonization.

PRRX1 Expression Is Associated with Good Prognosis and Metastasis-Free Disease

Our data from the studies in mice indicate that the loss of PRRX1 is associated with the development of metastases. Therefore, we wanted to know whether there was any relationship between the level of *PRRX1* expression and metastasis in human patients. We analyzed publically available data sets and found that low *PRRX1* transcription was associated with a poor relapse-free survival (RFS) in breast adenocarcinoma (Chin et al., 2006) (Figure 8A) and lung squamous cell carcinoma (SCC) (Raponi et al., 2006) (Figure 8A). Furthermore, low expression of both *PRRX1* and *TWIST1* associate with a lower RFS in lung SCC (Figure 8B). In contrast, there was no association between RFS and expression of *TWIST1* alone or of *SNAI1* (Figure S5A).

Consistent with our data in embryos and cancer cell lines, a statistically significant association was found between *PRRX1* and *TWIST1* expression in human breast adenocarcinoma and in two series of lung SCC (Chin et al., 2006; Raponi et al., 2006; Larsen et al., 2007) (Figure 8C). Similarly, and again as in embryos and tumor cells, no association was found between *PRRX1* and *SNAI1* expression (Figure 8C). Furthermore, significant correlations were evident between strong *PRRX1* expression and increased RFS either alone or in

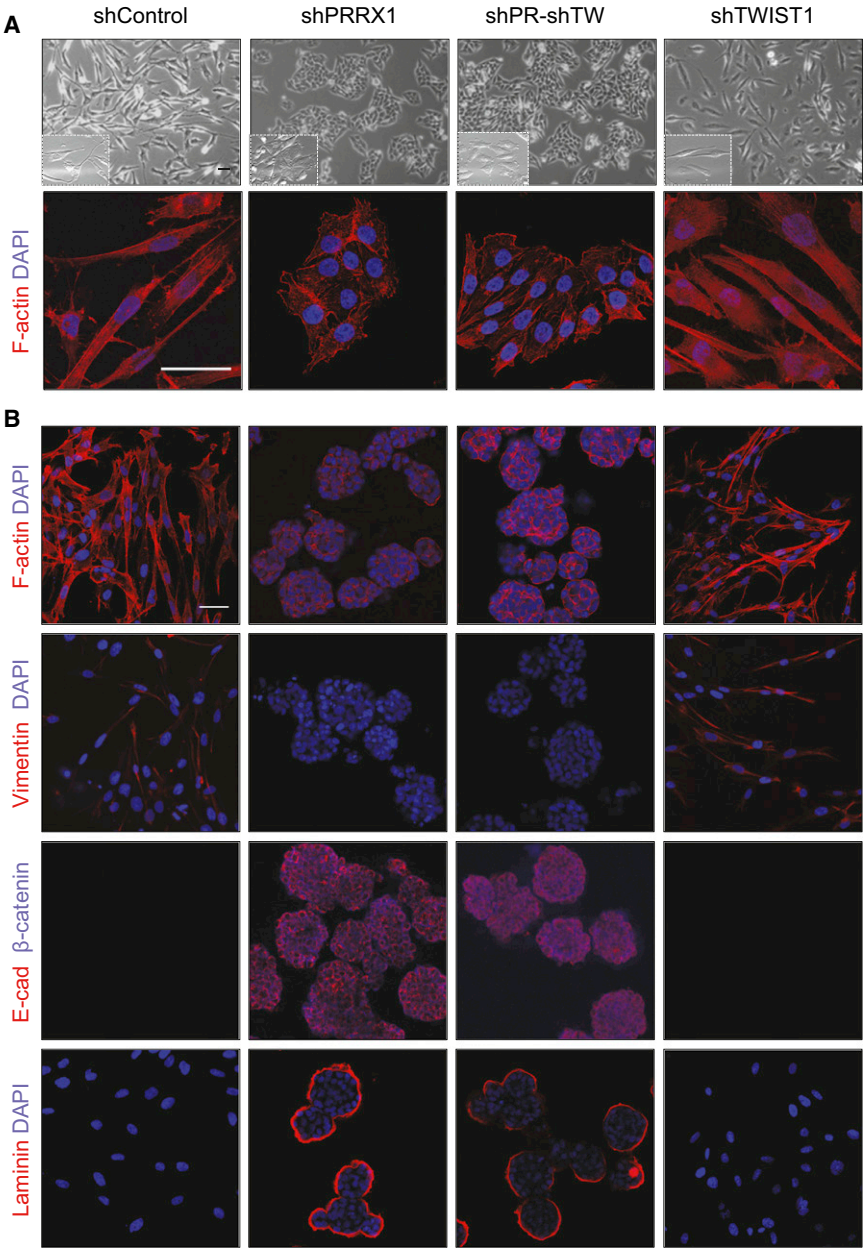

Figure 5. PRRX1 Knockdown in Cancer Cells Induces a Mesenchymal-to-Epithelial Transition and Spheroid Formation

(A) Phase-contrast and phalloidin staining images showing the phenotype of BT-549 cells transfected with indicated shRNAs. Scale bars: 50 μm. (B) Confocal images depicting the phenotype of the different BT-549 cells transfected with indicated shRNAs grown in 3D matrigel cultures and assessed for the presence of epithelial (E-cadherin and β-catenin), mesenchymal (vimentin), and extracellular matrix (laminin I) markers. DAPI staining (blue) was used as a nuclei reporter. Scale bar: 50 μm. PR, PRRX; TW, TWIST.

combination with *TWIST1* expression in breast carcinoma using a Log-rank-p-value method in the breast and lung series mentioned and in an additional breast series (Pawitan et al., 2005). The analysis of the Ur-Rehman (2011) data set available at the Online Breast Cancer Knowledgebase (ROCK) (Experimental Procedures) including 1570 human samples (Table S1) confirmed these findings.

We also observed a statistical correlation between *PRRX1* downregulation and progression to the metastatic disease. Analyzing the Chin's breast adenocarcinoma data set (Chin et al., 2006) we found that remarkably, metastasis did not develop in close to 90% of the tumors with medium/strong *PRRX1* expression (Figure 8D). The combination of strong *TWIST1* expression with strong *PRRX1* expression did not increase the percentage of metastasis-free tumors.

Finally, after the analyses of the different data sets, we examined the expression of *PRRX1* in 113 high-grade infiltrating breast ductal carcinoma (IDC) included in a tissue microarray (TMA). We found that around one third of the tumors analyzed showed significant *PRRX1* expression (Figures 8E and S5B) and interestingly, that metastasis did not develop in over 90% of these tumors (Figure 8F). These data are fully consistent with those found in our analyses of the data sets mentioned above. Thus, considering that all the data sets and the tissue microarrays used correspond to primary tumors, our observations indicate that strong *PRRX1* expression could be considered as an independent marker of good disease prognosis.

DISCUSSION

We have identified an EMT inducer that can trigger the full process in living embryos and human cancer cells. There are several features that make Prrx1 unique when compared to other well-known EMT-TFs, which expand our understanding of the complexity underlying metastatic processes, and help to reconcile conflicting results that have challenged the significance of EMT and stemness.

Prrx1 induces EMT in a manner independent of Snail1. Both during embryonic development and tumor progression, a temporal activation hierarchy drives the onset and maintenance of the mesenchymal program, with Snail1 situated high in the list. While Snail1 is required for the triggering of the EMT, other EMT-TFs reinforce and maintain the mesenchymal state (Peinado et al., 2007; Olmeda et al., 2008; Casas et al., 2011; Tran et al., 2011). However, we found that Snail1 does not influence *Prrx1* expression nor does Prrx1 modulate the expression of *Snail1*. Interestingly, we have observed that the same signaling molecule induces *Prrx1* and *Snail1* either in the embryo (BMP) or in epithelial cells (TGF-β). Hence, a single signal can

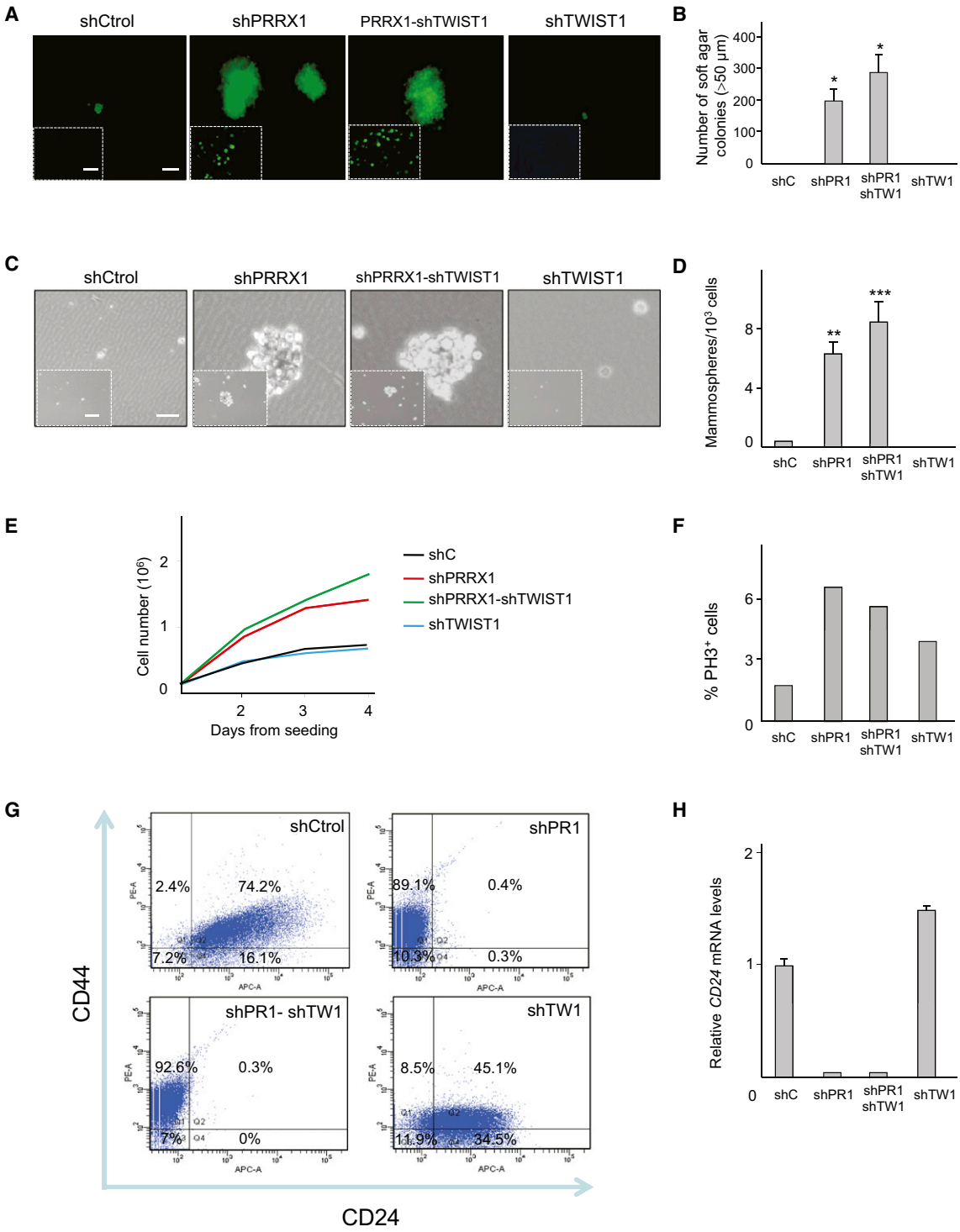

Figure 6. PRRX1 Knockdown Induces the Acquisition of Stem Cell Properties in Cancer Cells

(A) Representative fluorescence images showing the ability to induce colony formation in soft agar 15 days after seeding. Insets are low magnification images. Scale bars: 100 μm (main pictures) and 500 μm (inset).

(B) Quantification of soft agar colonies above 50 μm in diameter. Histograms represent the mean ± SD of three independent experiments (*$p < 0.05$, compared to the control condition).

(C) Phase-contrast images showing the mammosphere-forming capacity of different BT-549 cells. Scale bars: 50 μm (main pictures) and 200 μm (inset).

(D) Quantification of secondary mammospheres as the number formed/10^3 cells seeded. Histograms represent the mean ± SD of three independent experiments (**$p < 0.01$; ***$p < 0.001$ compared to the control condition).

(E) Growth curve of different BT-549 cells. Graphics shows a representative experiment (n = 3).

simultaneously and independently activate Prrx1 and Snail1 expression, and therefore, trigger parallel and probably nonredundant EMT pathways.

Our data show that Prrx1 is essential for the acquisition of invasive properties and indeed, when silenced in embryos, lpm cells fail to migrate. Similarly, there is no sign of cellular or local invasion in primary tumors generated by PRRX1-deficient BT-549 cells, even though both lpm cells and PRRX1-deficient human cells still express other EMT-TFs, including Twist1. Our data show that Prrx1 is essential for the acquisition of invasive properties and that Prrx1 cooperates with Twist1 in driving invasion in embryos and cancer cells. This is consistent with the described role of Twist in invasion and particularly, in the formation of invadopodia (Yang et al., 2004; Eckert et al., 2011). Once more, these findings support the cooperation between EMT-TFs, both during development and in cancer (Olmeda et al., 2008; Tran et al., 2011). Our data also reinforce the concept that EMT is important for the invasive behavior of the primary tumor, generating individual delaminating cells and subsequent tumor progression. Indeed, the loss of PRRX1 in BT-549 cells results in the formation of primary tumors without invasion and distant metastasis when orthotopically injected in the inguinal mammary fat pads. This is in agreement with the finding that abrogating classical EMT-TFs such as Snail1and Snail2 prevents individual cell migration and therefore attenuates invasion and subsequent distant metastasis when tested in similar experiments (Olmeda et al., 2008). Interestingly, albeit not commonly, lymph node metastases were found in PRRX1-TWIST1-deprived cells, consistent with the proposal that the EMT is not required for lymph node metastasis (Giampieri et al., 2009), albeit individual cells generated by EMT can also populate the lymph nodes.

A crucial difference between Prrx1 and other EMT-TFs is that Prrx1-induced EMT does not concur with the described induction of stem cell-like properties concomitant with Snail-, Twist-, or Zeb-mediated mesenchymal transitions (Mani et al., 2008; Morel et al., 2008; Wellner et al., 2009). On the contrary, it is PRRX1 loss rather than gain in cancer cells that is accompanied by the acquisition of stemness-related capabilities, including anchorage-independent growth, mammosphere formation, increased cell proliferation, and the conversion from a mostly $CD44^{+}/CD24^{+}$ double-positive population to $CD44^{high}$ single-positive cells. $CD44^{high}/CD24^{low}$ is the described profile for breast cancer stem cells associated with the most aggressive and metastatic types (Marotta et al., 2011).

Importantly, the loss of PRRX1 in mesenchymal cancer cells induces a complete reversion to the epithelial phenotype, even in the presence of classical EMT inducers. As such, our data show that abrogation of the EMT is important for metastatic colonization and this phenotype reversion concurrent with the aforementioned acquisition of stem cell-like properties upon PRRX1 downregulation favors metastatic colonization. This observation is similar to the finding that the MET process is essential for fibroblasts to acquire stem cell properties during cellular reprogramming (Li et al., 2010, Samavarchi-Tehrani et al., 2010), linking MET and stemness rather than EMT and stemness as described during the mesenchymal transition triggered by classical EMT-TFs. Our data also show that EMT and stemness can be independently regulated, but it is clear that they can coexist in some contexts such as in the migrating cancer stem cells and in early embryonic development. Indeed, EMT can induce the loss of epithelial characteristics of trophoblast stem cells while maintaining self-renewal and pluripotency (Abell et al., 2011), as shown for the classical EMT-TFs during tumor progression. However, it is worth noting that Snail2 (Slug) and Sox9 cooperate in the acquisition of the mesenchymal mammary stem cell state, with Snail2 essentially inducing the EMT and Sox9 facilitating entry into the stem cell state (Guo et al., 2012). All these findings indicate that EMT-TFs, or at least, the mesenchymal phenotype and stemness can coexist, as initially proposed following studies on colon carcinomas from which the concept of "migrating cancer stem cells" arose (Brabletz et al., 2005). However, the coexistence of these combined traits also implies phenotypic plasticity, because our data indicate that mesenchymal cells must revert to the epithelial phenotype to form the typical well-differentiated metastases while maintaining stemness, as suggested previously (Chaffer et al., 2006; Dykxhoorn et al., 2009; Celià-Terrassa et al., 2012; Brabletz, 2012). If MET is required for metastatic colonization, the loss of classical EMT-TFs would also convey the potential loss of stem cell properties associated with tumor-initiating capacity, thereby impairing metastatic colonization. Our findings showing that *PRRX1* loss induces both MET and stemness, and provides a mechanism that favors metastatic progression.

The fact that EMT and stemness are uncoupled in PRRX1-induced EMT again supports the existence of a parallel nonredundant EMT pathway mediated by PRRX1 in cancer cells and the requirement of PRRX1 loss for the development of distant macrometastases. As already mentioned, PRRX1 loss promotes stemness, thereby favoring tumor-initiating capacities when PRRX1 itself and the other EMT-TFs are downregulated after extravasation at the secondary organ to favor MET. By contrast, high PRRX1 expression can preclude progression to the metastatic state due to both a deficiency in tumor-initiating capacity and the persistence of an EMT state. As such, the unique association of strong PRRX1 expression in primary tumors with metastatic-free disease and good RFS in patients with different types of carcinoma, such as breast adenocarcinomas and lung SCC supports this proposal. On the one hand this suggests that strong PRRX1 expression in primary tumors could be used as diagnostic of good prognosis and on the other hand, that therapies aimed at targeting EMT might in fact promote metastatic colonization once cells have already delaminated from the primary tumor. Finally, the independent regulation of EMT

(F) Quantification of cells undergoing mitosis as assessed by PH3 staining 16 hr after cell seeding. Histograms shows a representative experiment (n = 3).
(G) BT-549 control cells and those in which PRRX1, TWIST1, or both had been downregulated were evaluated for their surface expression of CD44 and CD24 by FACS.
(H) *CD24* transcript levels observed in BT-549 control cells or in those where PRRX1, TWIST1 or both were downregulated. Histograms represent the mean ± SD of three independent experiments.
C or Ctrol, control; PR, PRRX; TW, TWIST.

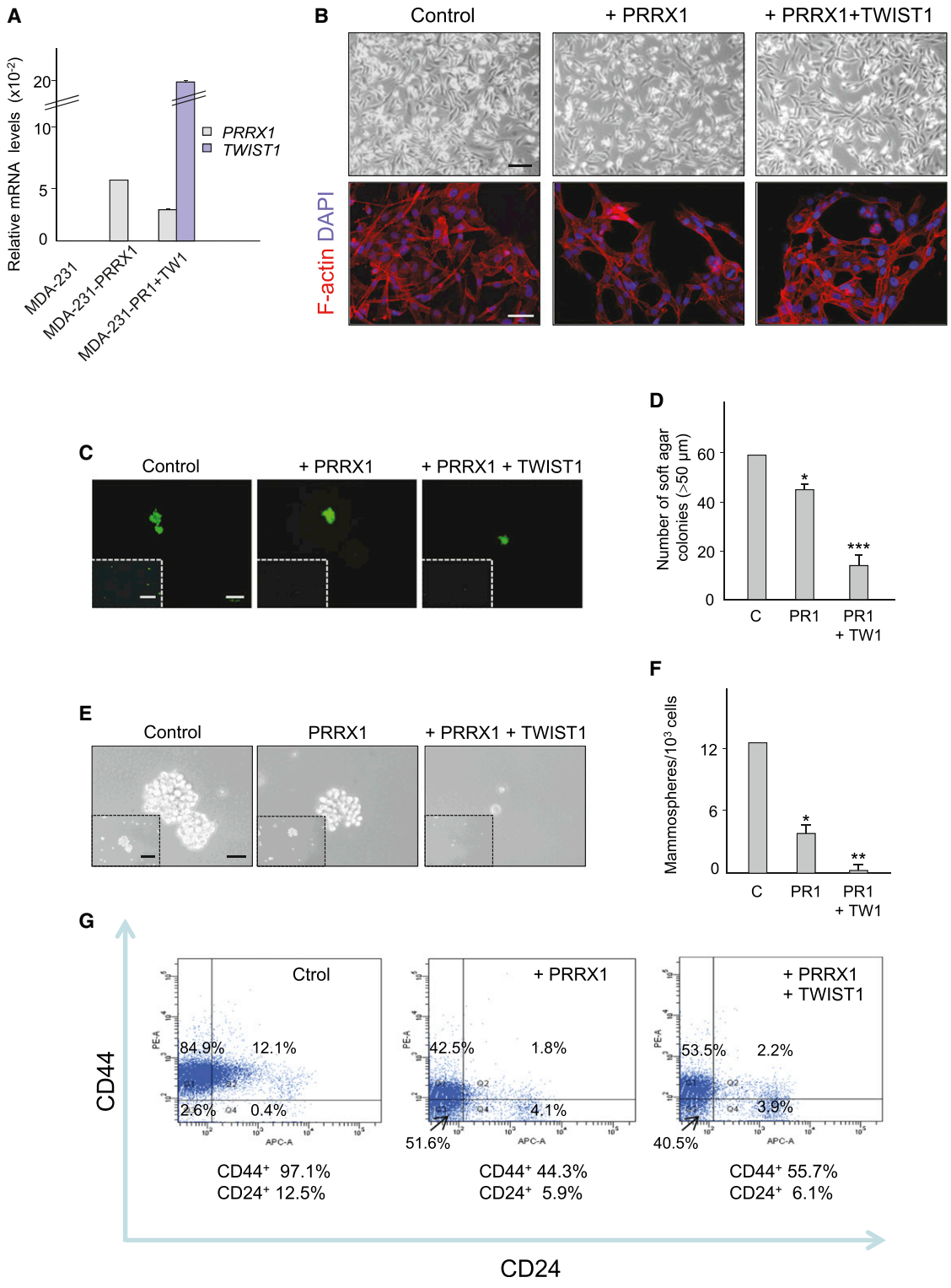

Figure 7. PRRX1 Ectopic Expression Impairs Stem Cell Properties in Cancer Cells

(A) Relative expression of *PRRX1* and *TWIST1* in MDA-231 control cells and in those transduced with viruses to ectopically express either PRRX1 or PRRX1 plus TWIST1. One representative of three independent experiments is shown and includes the mean ± SD of technical triplicates.

(B) Phase-contrast and phalloidin staining images showing the phenotype of control MDA-231 cells or of those in which PRRX1 has been ectopically expressed alone or together with TWIST1. Scale bars: 100 μm (upper panel) and 50 μm (lower panel).

(C) Representative fluorescence images showing the ability of MDA-231 control cells and that of those with ectopic expression of PRRX1 or PRRX1 plus TWIST1 to form colonies in soft agar 30 days after seeding. Insets are low magnification images. Scale bars: 100 μm (main pictures) and 500 μm (inset).

and stem cell properties supports the development of therapeutic strategies aimed at targeting stemness.

EXPERIMENTAL PROCEDURES

Human Breast Cancer

The analysis of *PRRX1* expression was performed using a total of 113 retrospective IDC from the Pathology Department of MD Anderson Cancer Center (MDACC) Madrid, Spain. All samples were grade 3. Patients underwent surgery between 2005 and 2006. Two different tumor areas from each sample were included into a tissue microarray (TMA) according to manufacturer's procedures. The mean patient age at surgery was 57.2 years (range, 38–85 years). The *HsPRRX1* probe was amplified by PCR from total cDNA and subcloned into a pGEMT-easy vector (Promega). In situ hybridization (ISH) of TMA sections was performed as described previously (Nieto et al., 1996) with some modifications. Briefly, 5 μm sections were deparaffinized in xylene and rehydrated in descending ethanol series. Slides were permeabilized with 10 ug/ml of proteinase K for 5 min at room temperature and prehybridized in hybridization buffer without probe for 3 hr and incubated with digoxigenin-labeled riboprobe overnight at 60°C. The following day, sections were washed in 2X SSC/50% formamide for 4 hr at 60°C. Hybridized probes were detected using an alkaline phosphatase-conjugated anti-digoxigenin antibody (Roche, 1:1000) in the presence of substrate nitroblue tetrazolium (NBT) 5-bromo-4-chloro-3-indolyl phosphate (BCIP) to produce a blue precipitate at the site of hybridization. Sections were photographed under a Leica DMR microscope (Leica, Wetzlar, Germany).

This study was performed following standard ethical procedures of the Spanish regulation (Ley de Investigación Orgánica Biomédica, 14 July 2007). All participants in this study gave written informed consent, and the study was approved by the Institutional Review Boards of MDACC Madrid.

Embryos

AB and Tup-Lof wild-type zebrafish strains were maintained at 28°C under standard conditions and the embryos were staged as described previously (Kimmel et al., 1995). Fertilized hen eggs were purchased from the Granja Gilbert (Tarragona, Spain) and incubated in a humidified incubator at 37.5°C. Chick embryos were staged according to Hamburger and Hamilton, 1951 (HH).

Cell Lines

MCF7, MDA-MB-231, MDA-MB-435S, A375P, HBL-100, MDA-MB-468, SKBR3, and BT-549 human tumor cell lines and MDCK dog kidney cells were purchased from the ATCC (Virginia, USA) and were cultured as described in Supplemental Experimental Procedures. The names of MDA cell lines have been reduced in the text for convenience.

Electroporation of Chicken Embryos and BMP2 Treatment

Chick embryos were electroporated with different expression constructs at stage HH4 as described previously (Acloque et al., 2011). In all experiments, the nonelectroporated side of the embryo served as a control. Human recombinant BMP2 protein (obtained from R&D Systems) was loaded onto heparin acrylic beads at a concentration of 0.2 mg/ml. See also Supplemental Experimental Procedures.

Morpholino Oligonucleotide and mRNA Injections

All MOs were obtained from Gene Tools and they were used as described elsewhere (Nasevicius and Ekker, 2000). The dose was chosen after testing the efficiency of MO1 in preventing splicing (Figure S3). The specificity of the MOs was checked by cloning the MO sequence in front of the EGFP coding sequence and assessing the decrease in GFP expression after coinjection with the corresponding MO. For overexpression analyses, embryos were injected with mRNAs synthesized for *prrx1a* coding sequence. Rescue experiments were performed by coinjecting mRNA plus MOs. See Supplemental Experimental Procedures for details.

Whole-Mount In Situ Hybridization

Whole-mount ISH was carried out essentially as described previously (Nieto et al., 1996). See Supplemental Experimental Procedures for details of the probes used.

Viral Production and Cell Infections

Human cDNA containing the coding sequence of *PRRX1* was subcloned in the pBABE-neo retroviral vector. Retroviral production and infection were carried out as previously described (Mani et al., 2008). After infection, MDA-231 or HBL-100 cells expressing either pBabe-neo (empty vector) or pBabe-neo-PRRX1 were selected with 400 μg/ml G418 for 2 weeks. The lentiviral vector containing the human *TWIST1* ORF sequence was obtained from Open Biosystems (OHS5898-101004920). Lentiviral plasmids containing shRNAs were purchased from Open Biosystems and are listed as the following: Human shPRRX1 (RHS3979-9588052 and RHS3979-9588055), and Human shTWIST1 (RHS3979-9587949 and RHS3979-9587951). Lentiviral supernatants were produced using a viral packaging system that includes the psPAX2 and pM2DG plasmids (purchased from Open Biosystems). Two days after transfection, the viral supernatants were collected and used to infect BT-549 and MDA-231 cells, which were then selected with 2 μg/ml puromycine. The empty pLKO.1 vector was used as a control and in all cases, the cells were also infected with the empty pGIPZ vector (obtained from Open Biosystems) as a reporter of EGFP expression. For BT-549 cells, at least two independent pools were generated in each case and the cultured cells were initially tested for changes in morphology, expression, and invasive properties. Different pools behaved similarly and for each condition, one was chosen for the in vivo experiments.

Total RNA Extraction, cDNAs Isolation, and QRT-PCR Analysis

All the protocols are described in detail in the Supplemental Experimental Procedures.

Generation and Characterization of Prrx1-Expressing Stable Cell Lines

Stable transfectants were generated in MDCK cells and selected for 2 weeks with 400 μg/ml G418. Five independent clones were analyzed for pcDNA3-mPrrx1 and three for pcDNA3 alone (mock). Where indicated, cells were transfected with siRNAs using Lipofectamine RNAiMAX according to the manufacturer's instructions (Invitrogen). Three independent siRNA sequences were tested. See Supplemental Experimental Procedures for more details and primer sequences.

Immunofluorescence

The methods used are described in the Supplemental Experimental Procedures.

Tumor Growth and Histologic Studies

Mouse studies were carried out with the approval of the IDIBELL Animal Ethics Committee (Procedure 4587 AFF) and in accordance with the Spanish National Health and Medical Research Council's guidelines and the AALAC for the care and use of laboratory animals. Details are provided in the Supplemental Experimental Procedures.

(D) Quantification of soft agar colonies above 50 μm in diameter. Histograms represent the mean ± SD of three independent experiments (*$p < 0.05$, ***$p < 0.001$ compared to the control condition).
(E) Phase-contrast images showing the ability to form mammospheres of the different MDA-231 cells. Scale bars: 50 μm (main pictures) and 200 μm (inset).
(F) Quantification of tertiary mammospheres as the number formed/10^3 cells seeded. Histograms represent the mean ± SD of three independent experiments (*$p < 0.05$; **$p < 0.01$ compared to the control condition).
(G) Analysis of CD44 and CD24 surface expression by FACS.
C, control; PR, PRRX; TW, TWIST.

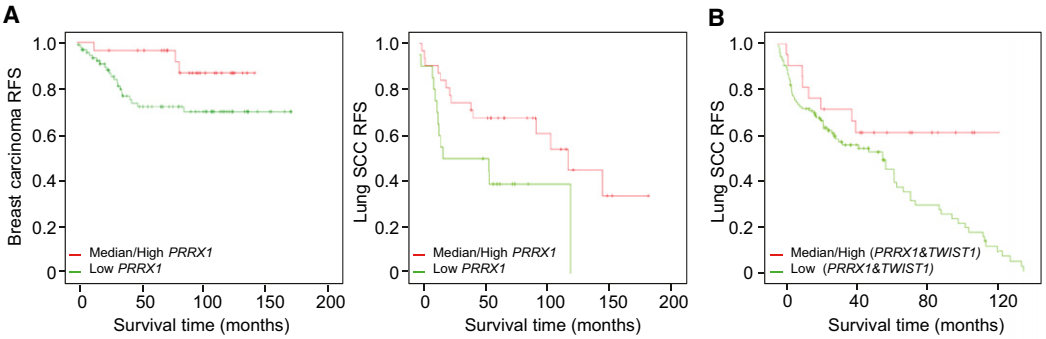

C

PRRX1 expression *n (%)	LOW	MEDIAN/HIGH
Breast dataset Chin et al., 2006		
***TWIST1* expression** LOW (n=74) MEDIAN/HIGH (n=43)	23 (31.1) 6 (13.9)	51 (68.9) 37 (86.1) p=0.033
***SNAI1* expression** LOW (n=38) MEDIAN/HIGH (n=79)	10 (26.3) 19 (24.1)	28(73.3) 60(75.9) ns
Lung dataset Raponi et al., 2006		
***TWIST1* expression** LOW (n=95) MEDIAN/HIGH (n=33)	76 (80.0) 12 (36.4)	19 (20.0) 21(63.6) p<0.001
***SNAI1* expression** LOW (n=88) MEDIAN/HIGH (n=40)	63(71.6) 25(62.5)	25(28.4) 15(37.5) ns
Lung dataset Larsen et al., 2007		
***TWIST1* expression** LOW (n=24) MEDIAN/HIGH (n=27)	13(54.2) 7(25.9)	11(45.8) 20(74.1) p=0.039
***SNAI1* expression** LOW (n=29) MEDIAN/HIGH (n=22)	10 (34.5) 10 (45.5)	19 (65.5) 12 (54.5) ns

D

	METASTASIS NO	METASTASIS YES
Breast dataset Chin et al., 2006		
***PRRX1* expression** LOW (n=29) MEDIAN/HIGH (n=88)	7 (24.1) **77 (87.5)**	22 (75.9) 11 (12.5) p=0.027

	METASTASIS NO	METASTASIS YES
Breast dataset Chin et al, 2006		
***PRRX1* and *TWIST1* expression** LOW (n=32) MEDIAN/HIGH (n=85)	8 (25) **76 (89.4)**	24 (75) 9 (10.6) p<0.001

E

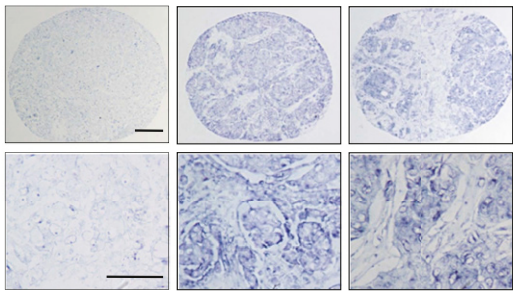

F

	METASTASIS NO	METASTASIS YES
TMA MD-Anderson		
***PRRX1* expression** Negative (n=78) Positive (n=35)	60 (76.9) **32 (91.4)**	18 (23.1) 3 (8.6) p=0.05

Figure 8. Strong PRRX1 Expression in Breast Carcinomas and Lung SCC Is Correlated with the Lack of Metastases and Increased RFS

(A) Kaplan-Meier plots showing the association between *PRRX1* expression and RFS using data sets from the Chin breast adenocarcinoma series (Chin et al., 2006) and from a series of lung SCC (Raponi et al., 2006).

(B) Kaplan-Meier plots showing the association between combined high *PRRX1* and high *TWIST1* expression with increased RFS from the lung SCS database in (A).

(C) Correlation between *PRRX1* and *TWIST1* expression in a breast adenocarcinoma and two independent lung SCC data sets.

(D) Statistical association between either *PRRX1* alone or *PRRX1* and *TWIST1* together with metastasis.

(E) Representative examples of ISH for *PRRX1* in a retrospective grade 3 infiltrating ductal breast carcinoma series (n = 113) included in a tumor microarray (TMA). Lower panels show high power images. Scale bars: 200 μm (upper panels) and 50 μm (lower panels).

(F) Statistical association between *PRRX1* expression and metastasis formation from the expression analysis of the TMA shown in (E).

*n (%), number of cases (percentage); ns, nonsignificant.

See also Figure S5 and Table S1.

Migration and Invasion Assays

For migration assays cells were seeded in six-well culture dishes at a density of 1×10^6 cells/well. A wound was made in the center of the culture 24 hr later, and phase-contrast pictures were taken at different intervals. Invasion assays on collagen type-IV gels were performed as described previously (Cano et al., 2000). Briefly, 35,000–50,000 cells of each type were seeded onto the upper surface of the filters in modified Boyden chambers. After 7 or 16 hr incubation for BT-549 and HBL-100 respectively, cells attached to the lower part of the filters were fixed in methanol, stained with 4,6-diamidinophenylindole (DAPI), and counted. Longer incubation times for HBL-100 cells were required because they are noninvasive.

Soft Agar Assays and Mammosphere Cultures

For details, see the Supplemental Experimental Procedures.

Cell Proliferation and Cell Cytometry Analysis

Analyses of cell proliferation and cell cytometry were carried out as described in the Supplemental Experimental Procedures.

Metanalysis

To validate the metastatic prediction model, several independent data sets of breast carcinoma (See Chin et al., 2006; Pawitan et al., 2005) and lung SCC series (Raponi et al., 2006; Larsen et al., 2007) were analyzed. The breast and lung microarrays, and the clinical data were obtained from ICR and GEO databases, respectively. In addition, the Ur-Rehman data set, publicly available in ROCK (http://www.rock.icr.ac.uk) was also used in the analysis. The Ur-Rehman data set was a collection of independent published breast cancer data sets containing 1,570 samples analyzed with the U133 Affymetrix platform arrays, all of them were normalyzed using the same Robust Multi-array Average method. The statistical survival analysis associated to the breast and lung samples was performed using ROCK (http://www.rock.icr.ac.uk) and SPSS software (SPSS), respectively. Kaplan-Meier plots of the RFS curves are represented using log-rank tests. The expression values of *PRRX1, TWIST1*, and *SNAI1* was categorized using upper quartile (25% against rest). The Chi-square contingency test Yates correction, or Fisher's exact test, was used to determine the statistical significance of the relationships between *PRRX1* expression and *TWIST1* expression, and metastasis. Values of $p < 0.05$ were considered statistically significant. These analyses were carried out using the SPSS 17.0 for statistical software.

SUPPLEMENTAL INFORMATION

Supplemental Information includes five figures, one table, and Supplemental Experimental Procedures and can be found with this article online at http://dx.doi.org/10.1016/j.ccr.2012.10.012.

ACKNOWLEDGMENTS

We would like to thank members of Angela Nieto's lab for their helpful suggestions, Antonio Caler for the flow cytometry analyses, Antònia Vinyals for her help with the cell extravasation experiments, Diana Abad for excellent care of the zebrafish facility, and Giovanna Exposito for her invaluable assistance with the confocal microscopes. This work has been supported by grants from the Spanish Ministry of Science and Innovation BFU2008-01042 (to M.A.N.), SAF2010-21143 (to A.C.), and CONSOLIDER-INGENIO 2010 CSD2007-00017 to both labs. A grant from the Spanish Fondo de Investigaciones Sanitarias (FIS PS09/00373) supports Á.F.'s lab and CONSOLIDER-INGENIO 2010 CSD2007-00023 and Generalitat Valenciana (Prometeo 2008/049 and ISIC/2012/010) also support M.A.N.'s lab.

Received: June 7, 2012
Revised: September 17, 2012
Accepted: October 22, 2012
Published online: November 29, 2012

REFERENCES

Abell, A.N., Jordan, N.V., Huang, W., Prat, A., Midland, A.A., Johnson, N.L., Granger, D.A., Mieczkowski, P.A., Perou, C.M., Gomez, S.M., et al. (2011). MAP3K4/CBP-regulated H2B acetylation controls epithelial-mesenchymal transition in trophoblast stem cells. Cell Stem Cell *8*, 525–537.

Acloque, H., Ocaña, O.H., Matheu, A., Rizzoti, K., Wise, C., Lovell-Badge, R., and Nieto, M.A. (2011). Reciprocal repression between Sox3 and snail transcription factors defines embryonic territories at gastrulation. Dev. Cell *21*, 546–558.

Brabletz, T. (2012). To differentiate or not—routes towards metastasis. Nat. Rev. Cancer *12*, 425–436.

Brabletz, T., Jung, A., Spaderna, S., Hlubek, F., and Kirchner, T. (2005). Opinion: migrating cancer stem cells - an integrated concept of malignant tumour progression. Nat. Rev. Cancer *5*, 744–749.

Cano, A., Pérez-Moreno, M.A., Rodrigo, I., Locascio, A., Blanco, M.J., del Barrio, M.G., Portillo, F., and Nieto, M.A. (2000). The transcription factor snail controls epithelial-mesenchymal transitions by repressing E-cadherin expression. Nat. Cell Biol. *2*, 76–83.

Casas, E., Kim, J., Bendesky, A., Ohno-Machado, L., Wolfe, C.J., and Yang, J. (2011). Snail2 is an essential mediator of Twist1-induced epithelial mesenchymal transition and metastasis. Cancer Res. *71*, 245–254.

Celià-Terrassa, T., Meca-Cortés, O., Mateo, F., de Paz, A.M., Rubio, N., Arnal-Estapé, A., Ell, B.J., Bermudo, R., Díaz, A., Guerra-Rebollo, M., et al. (2012). Epithelial-mesenchymal transition can suppress major attributes of human epithelial tumor-initiating cells. J. Clin. Invest. *122*, 1849–1868.

Cserjesi, P., Lilly, B., Bryson, L., Wang, Y., Sassoon, D.A., and Olson, E.N. (1992). MHox: a mesodermally restricted homeodomain protein that binds an essential site in the muscle creatine kinase enhancer. Development *115*, 1087–1101.

Chaffer, C.L., Brennan, J.P., Slavin, J.L., Blick, T., Thompson, E.W., and Williams, E.D. (2006). Mesenchymal-to-epithelial transition facilitates bladder cancer metastasis: role of fibroblast growth factor receptor-2. Cancer Res. *66*, 11271–11278.

Chin, K., DeVries, S., Fridlyand, J., Spellman, P.T., Roydasgupta, R., Kuo, W.L., Lapuk, A., Neve, R.M., Qian, Z., Ryder, T., et al. (2006). Genomic and transcriptional aberrations linked to breast cancer pathophysiologies. Cancer Cell *10*, 529–541.

Dykxhoorn, D.M., Wu, Y., Xie, H., Yu, F., Lal, A., Petrocca, F., Martinvalet, D., Song, E., Lim, B., and Lieberman, J. (2009). miR-200 enhances mouse breast cancer cell colonization to form distant metastases. PLoS ONE *4*, e7181.

Eckert, M.A., Lwin, T.M., Chang, A.T., Kim, J., Danis, E., Ohno-Machado, L., and Yang, J. (2011). Twist1-induced invadopodia formation promotes tumor metastasis. Cancer Cell *19*, 372–386.

Giampieri, S., Manning, C., Hooper, S., Jones, L., Hill, C.S., and Sahai, E. (2009). Localized and reversible TGFbeta signalling switches breast cancer cells from cohesive to single cell motility. Nat. Cell Biol. *11*, 1287–1296.

Guo, W., Keckesova, Z., Donaher, J.L., Shibue, T., Tischler, V., Reinhardt, F., Itzkovitz, S., Noske, A., Zürrer-Härdi, U., Bell, G., et al. (2012). Slug and Sox9 cooperatively determine the mammary stem cell state. Cell *148*, 1015–1028.

Gupta, G.P., and Massagué, J. (2006). Cancer metastasis: building a framework. Cell *127*, 679–695.

Hamburger, V., and Hamilton, H. (1951). A series of normal stages in the development of the chick embryo. J. Morphol. *88*, 49–92.

Kimmel, C.B., Ballard, W.W., Kimmel, S.R., Ullmann, B., and Schilling, T.F. (1995). Stages of embryonic development of the zebrafish. Dev. Dyn. *203*, 253–310.

Larsen, J.E., Pavey, S.J., Passmore, L.H., Bowman, R., Clarke, B.E., Hayward, N.K., and Fong, K.M. (2007). Expression profiling defines a recurrence signature in lung squamous cell carcinoma. Carcinogenesis *28*, 760–766.

Li, R., Liang, J., Ni, S., Zhou, T., Qing, X., Li, H., He, W., Chen, J., Li, F., Zhuang, Q., et al. (2010). A mesenchymal-to-epithelial transition initiates and is required for the nuclear reprogramming of mouse fibroblasts. Cell Stem Cell *7*, 51–63.

Mani, S.A., Guo, W., Liao, M.J., Eaton, E.N., Ayyanan, A., Zhou, A.Y., Brooks, M., Reinhard, F., Zhang, C.C., Shipitsin, M., et al. (2008). The epithelial-mesenchymal transition generates cells with properties of stem cells. Cell *133*, 704–715.

Marotta, L.L., Almendro, V., Marusyk, A., Shipitsin, M., Schemme, J., Walker, S.R., Bloushtain-Qimron, N., Kim, J.J., Choudhury, S.A., Maruyama, R., et al. (2011). The JAK2/STAT3 signaling pathway is required for growth of $CD44^{+}CD24^{-}$ stem cell-like breast cancer cells in human tumors. J. Clin. Invest. *121*, 2723–2735.

McKean, D.M., Sisbarro, L., Ilic, D., Kaplan-Alburquerque, N., Nemenoff, R., Weiser-Evans, M., Kern, M.J., and Jones, P.L. (2003). FAK induces expression of Prx1 to promote tenascin-C-dependent fibroblast migration. J. Cell Biol. *161*, 393–402.

Mejlvang, J., Kriajevska, M., Vandewalle, C., Chernova, T., Sayan, A.E., Berx, G., Mellon, J.K., and Tulchinsky, E. (2007). Direct repression of cyclin D1 by SIP1 attenuates cell cycle progression in cells undergoing an epithelial mesenchymal transition. Mol. Biol. Cell *18*, 4615–4624.

Morel, A.P., Lièvre, M., Thomas, C., Hinkal, G., Ansieau, S., and Puisieux, A. (2008). Generation of breast cancer stem cells through epithelial-mesenchymal transition. PLoS ONE *3*, e2888.

Moreno-Bueno, G., Salvador, F., Martín, A., Floristán, A., Cuevas, E.P., Santos, V., Montes, A., Morales, S., Castilla, M.A., Rojo-Sebastián, A., et al. (2011). Lysyl oxidase-like 2 (LOXL2), a new regulator of cell polarity required for metastatic dissemination of basal-like breast carcinomas. EMBO Mol. Med. *3*, 528–544.

Nasevicius, A., and Ekker, S.C. (2000). Effective targeted gene 'knockdown' in zebrafish. Nat. Genet. *26*, 216–220.

Nieto, M.A. (2011). The ins and outs of the epithelial to mesenchymal transition in health and disease. Annu. Rev. Cell Dev. Biol. *27*, 347–376.

Nieto, M.A., and Cano, A. (2012). The epithelial-mesenchymal transition under control: Global programs to regulate epithelial plasticity. Semin. Cancer Biol. *22*, 361–368.

Nieto, M.A., Patel, K., and Wilkinson, D.G. (1996). In situ hybridization analysis of chick embryos in whole mount and tissue sections. Methods Cell Biol. *51*, 219–235.

Olmeda, D., Montes, A., Moreno-Bueno, G., Flores, J.M., Portillo, F., and Cano, A. (2008). Snai1 and Snai2 collaborate on tumor growth and metastasis properties of mouse skin carcinoma cell lines. Oncogene *27*, 4690–4701.

Pawitan, Y., Bjöhle, J., Amler, L., Borg, A.L., Egyhazi, S., Hall, P., Han, X., Holmberg, L., Huang, F., Klaar, S., et al. (2005). Gene expression profiling spares early breast cancer patients from adjuvant therapy: derived and validated in two population-based cohorts. Breast Cancer Res. *7*, R953–R964.

Peinado, H., Olmeda, D., and Cano, A. (2007). Snail, Zeb and bHLH factors in tumour progression: an alliance against the epithelial phenotype? Nat. Rev. Cancer *7*, 415–428.

Prigent, C., and Dimitrov, S. (2003). Phosphorylation of serine 10 in histone H3, what for? J. Cell Sci. *116*, 3677–3685.

Raponi, M., Zhang, Y., Yu, J., Chen, G., Lee, G., Taylor, J.M., Macdonald, J., Thomas, D., Moskaluk, C., Wang, Y., and Beer, D.G. (2006). Gene expression signatures for predicting prognosis of squamous cell and adenocarcinomas of the lung. Cancer Res. *66*, 7466–7472.

Samavarchi-Tehrani, P., Golipour, A., David, L., Sung, H.K., Beyer, T.A., Datti, A., Woltjen, K., Nagy, A., and Wrana, J.L. (2010). Functional genomics reveals a BMP-driven mesenchymal-to-epithelial transition in the initiation of somatic cell reprogramming. Cell Stem Cell *7*, 64–77.

Sefton, M., Sánchez, S., and Nieto, M.A. (1998). Conserved and divergent roles for members of the Snail family of transcription factors in the chick and mouse embryo. Development *125*, 3111–3121.

Sleeman, K.E., Kendrick, H., Ashworth, A., Isacke, C.M., and Smalley, M.J. (2006). CD24 staining of mouse mammary gland cells defines luminal epithelial, myoepithelial/basal and non-epithelial cells. Breast Cancer Res. *8*, R7.

Thiery, J.P., Acloque, H., Huang, R.Y., and Nieto, M.A. (2009). Epithelial-mesenchymal transitions in development and disease. Cell *139*, 871–890.

Tran, D.D., Corsa, C.A., Biswas, H., Aft, R.L., and Longmore, G.D. (2011). Temporal and spatial cooperation of Snail1 and Twist1 during epithelial-mesenchymal transition predicts for human breast cancer recurrence. Mol. Cancer Res. *9*, 1644–1657.

Vega, S., Morales, A.V., Ocaña, O.H., Valdés, F., Fabregat, I., and Nieto, M.A. (2004). Snail blocks the cell cycle and confers resistance to cell death. Genes Dev. *18*, 1131–1143.

Wellner, U., Schubert, J., Burk, U.C., Schmalhofer, O., Zhu, F., Sonntag, A., Waldvogel, B., Vannier, C., Darling, D., zur Hausen, A., et al. (2009). The EMT-activator ZEB1 promotes tumorigenicity by repressing stemness-inhibiting microRNAs. Nat. Cell Biol. *11*, 1487–1495.

Yang, J., and Weinberg, R.A. (2008). Epithelial-mesenchymal transition: at the crossroads of development and tumor metastasis. Dev. Cell *14*, 818–829.

Yang, J., Mani, S.A., Donaher, J.L., Ramaswamy, S., Itzykson, R.A., Come, C., Savagner, P., Gitelman, I., Richardson, A., and Weinberg, R.A. (2004). Twist, a master regulator of morphogenesis, plays an essential role in tumor metastasis. Cell *117*, 927–939.